Strategies for Multi-Fidelity Optimization of Multi-Stage Compressors with Throughflow and 3D CFD

Markus Schnoes, Andreas Schmitz, Georgios Goinis, Christian Voß and Eberhard Nicke
markus.schnoes@dlr.de

Institute of Propulsion Technology
German Aerospace Center (DLR)
51147 Cologne, Germany

ABSTRACT

The aerodynamic design of turbomachinery is an exciting engineering problem that involves a vast design space and requires proficiency in multiple engineering disciplines. For multi-stage compressors, the large dimension of the design space arises from the geometric freedom to shape each blade row individually. Although the basis of most designs is formed by throughflow computations, the state-of-the art for aerodynamic evaluation is steady-state RANS. The computational expense for a single evaluation of a multi-stage machine with RANS is affordable, shape optimizations with hundreds of evaluations becomes expensive.

This paper presents two strategies to tackle these problems: Firstly, a novel airfoil family is employed that helps to reduce the number of design parameters. It was generated based on a parametric study of optimal airfoil shape for varying design requirements. Secondly, an optimizer is used that supports simultaneous evaluations of the objective function on multiple fidelity levels. Here, cheap throughflow calculations are conducted on the low-fidelity side and RANS is used on the high-fidelity side. Inside the optimizer, multi-fidelity support is enabled by a Co-Kriging surrogate model. This approach is expected to speed-up the optimization by guiding expensive evaluations of the 3D CFD setup into promising regions of the design space.

These strategies are assessed by testing different optimization setups for a four stage compressor. Both purely low and high-fidelity optimizations are conducted as well as multi-fidelity optimizations. In comparison to the baseline design, the isentropic efficiency predicted by RANS for the working line points on the 95% and the 100% speed line is increased by above 1.2%. The driving mechanism is a load redistribution between the stages that mainly reduces the shock strength of the second rotor.

NOMENCLATURE

Acronyms

ACDC	Advanced Compressor Design Code
CFD	Computational Fluid Dynamics
HF	High-fidelity
LF	Low-fidelity
RANS	Reynolds-averaged Navier-Stokes
SLC	Streamline curvature
VCC	Versatile Compressor Cascades

Greek letters

β	relative flow angle measured from axial direction
ω	total pressure loss coefficient
ρ	density
γ	blade stagger angle

Latin letters

a	profile area
c	blade chord length
DF	diffusion factor
h	enthalpy
M	Mach number
MVDR	$= (\rho_2 \mathrm{v}_{\mathrm{m},2})/(\rho_1 \mathrm{v}_{\mathrm{m},1})$, meridional velocity density ratio
Re	Reynolds number
s	blade pitch
U	rotational velocity
v	velocity

Sub- and superscripts

1	cascade inlet quantity
2	cascade outlet quantity
m	meridional direction
t	stagnation quantity
θ	circumferential direction
x	axial direction

INTRODUCTION

The typical turbomachinery design task starts with low-fidelity tools that are able to explore the design space and have short execution times. Many important design choices are made on this level of detail. In the field of compressor design, mean-line or throughflow codes are the methods of choice. Afterwards, detailed blade row design is conducted with steady-state RANS simulations.

With an increasing demand for efficient engines, the design space for turbomachinery is expanded continuously to more sophisticated designs. As an example, instead of stacking blades with profiles from classic airfoil families, a geometric description of blade shape with B-spline surfaces offers more freedom to decrease flow losses. For a low number of blade rows, mathematical optimization is common practice in the industry to find optimal blade shapes in these high dimensional parameter spaces.

Since the end of the 1980s, many studies have been carried out using preliminary design methods in combination with numerical optimization [1, 2, 3]. Conducting optimizations based on mean-line or throughflow computations sets high demands for the modeling which is heavily based on empirical correlations: In a manual optimization, an experienced designer modifies only a handful of pa-

rameters, sticking closely to a baseline design and he is aware of the flaws of the underlying model and knows how to interpret the results. An automated process in an optimization cannot offer such a differentiated assessment. For this reason, Casey [4] points out that in preliminary design performance prediction methods are not accurate enough to be used in numerical optimization. There is a chance that they lead to a disruptive new design, but most likely these are outside the range of model validity.

High-fidelity tool sets including 3D CFD describe the turbomachinery flow more generally and are able to assess designs outside the scope of experience. The studies [5, 6, 7] highlight the application of design optimization to a single row or stage. The simultaneous optimization of multiple stages with steady-state RANS simulation poses a very challenging problem due to high computation times and the curse of dimensionality. For these reasons, only few publications exist on the holistic optimization of multiple stages. Only recently, a detailed optimization of a four stage low pressure turbine with 350 degrees of freedom is presented in [8].

In the classic design process, the turbomachine is designed with an increasing level of simulation fidelity. According to this approach, in [3], the result of a throughflow optimization of a highly loaded fan is further evolved with a 3D CFD optimization. Instead of sequentially designing with an increasing level of model detail, in a multi-fidelity optimization multiple levels of fidelity are handled simultaneously: an algorithm chooses between the fast evaluations of a low-fidelity model and the detailed resolution of a high-fidelity model. This approach is expected to significantly speed-up the optimization by guiding the expensive evaluations of the high-fidelity setup into interesting regions. Internally, these methods can be implemented based on Co-Kriging surrogate models. An academic application of multi-fidelity is presented by Brooks [9]. In his work, a multi-fidelity optimization is compared with a conventional ordinary Kriging optimization. For this purpose Brooks et al. optimized the well-known NASA rotor 37 [10]. In order to ensure comparability, Brooks et al. provided the same computing budget and found out that the Co-Kriging model outperforms the Kriging model based only on high-fidelity data. An industrial application is presented by Lapworth et al. [11]. The authors come to the conclusion that multi-fidelity optimization achieves a higher increase in efficiency with the same computing time. The multi-fidelity tool set of this work was successfully employed for the complex optimization of a counter-rotating fan stage [12]. The aim of the optimization was to maximize the efficiency and minimize the sound pressure in the exit direction while complying with 15 constraints.

In the focus of this work is the optimization of a four stage transonic research compressor. The optimization setup is application-oriented and includes multiple objectives, multiple operating points and structural mechanics. While the above mentioned multi-fidelity papers use 3D CFD on the low and on the high-fidelity side, this work tries to combine throughflow and 3D CFD in a single optimization. To assess this approach, the optimization is conducted with setups using single as well as multiple fidelities. Additionally, this work employs a novel airfoil family to reduce the dimensionality of the design space. The airfoil family was generated in previous work [13] and is based on a parametric study of optimal airfoil shape for varying design requirements. Utilizing these airfoils restricts the overall design space, but it dramatically decreases the number of parameters necessary to describe a blade while ensuring low losses and wide working ranges on each blade section.

This work is structured as follows: at first, the compressor design system is present including the throughflow code and the optimization suite. Afterwards, the optimization setup for the re-design of the test compressor is introduced. And finally, the results of single-fidelity and multi-fidelity optimizations are given.

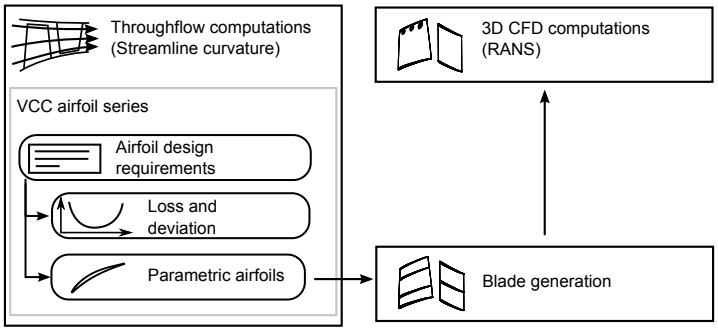

Figure 1: Design work flow for compressors

COMPRESSOR DESIGN SYSTEM

The design work flow for this paper is presented in figure 1. The new airfoil series is the foundation of the design system, it provides airfoil geometries and performance estimates in terms of loss and deviation. Using the throughflow code, airfoils are determined for each blade section in a design-point computation. Afterwards, the blade geometries can be constructed by stacking the airfoils to blades. On this basis, structural mechanics can be assessed and a 3D CFD setup can be generated. This section introduces the new airfoil series, the throughflow code and the numerical optimization environment.

Database of Optimized Airfoils

The airfoil series in this work is generated based on a parametric study on the geometry of optimal airfoils for a variation in geometric cascade parameters and design point operation conditions. The idea is adopted from Köller [14], extended to transonic airfoils and implemented into an overall design strategy. The variation parameters, denoted as "design requirements", form a seven dimensional requirement space: stagger angle γ, pitch-chord ratio $\frac{s}{c}$ and dimensionless airfoil cross-section area $\frac{a}{c^2}$, together with the design point properties inlet Mach number M_1, Reynolds number Re, streamtube contraction MVDR and aerodynamic loading based on the diffusion factor DF. Whereas, the diffusion factor is defined as:

$$DF = 1 - \frac{v_2}{v_1} + \frac{v_{1,\theta} - v_{2,\theta}}{2v_1}\frac{s}{c}. \tag{1}$$

The bounds for these design requirements are selected to cover the requirements of multi-stage axial compressors including transonic front and subsonic rear stages, thick hub and slender tip blade sections.

Around 2000 airfoils have been generated based on a design strategy for compressor airfoils at discrete points in this seven-dimensional requirement space. The design strategy employs numerical optimization and evaluates each candidate airfoil by computing the loss characteristic around the design point with MISES [15]. During the optimization, the airfoil shape is described with 14 design parameters that fix the control points of a B-spline representation of the blade. The objective is to find airfoil shapes with wide working ranges and low losses in the design point and over the majority of the incidence range. A set of constraints ensures the new airfoils fulfill structural requirements. For example, parameters like the position of the centroid and the shape of the thickness distribution are restricted.

Afterwards, optimal airfoils are available at discrete points in the requirement space. On this basis, interpolation and approximation routines can be used to create airfoils for new requirement sets, here Kriging [16] is chosen as interpolation scheme. This functional relation between design requirements and airfoil geometry defines the new airfoil series which is denoted as VCC (Versatile Compressor Cascades). The airfoil series was originally presented in [13], where the

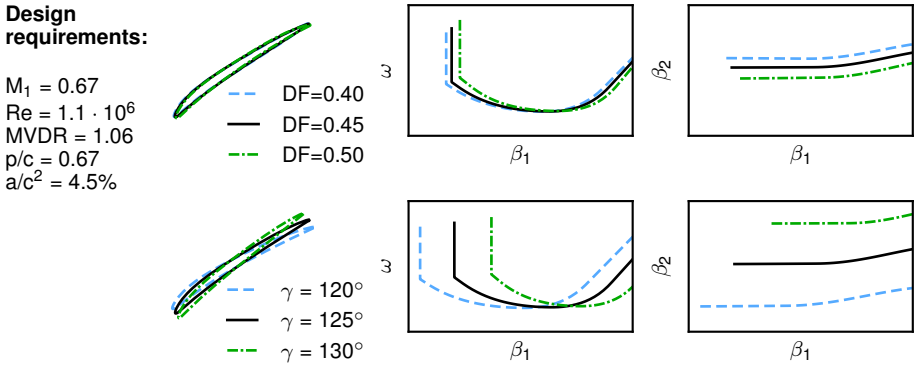

Figure 2: Sample variation of stagger angle and design diffusion factor for a stator airfoil inside the VCC airfoil series

performance of two transonic cascades is validated with RANS simulations. For two further subsonic cases the new airfoils have been compared to a Controlled Diffusion Airfoil (CDA) and a state-of-the-art stationary gas turbine airfoil.

For throughflow computations new loss and deviation correlations are generated for the airfoil series based on blade-to-blade computations with MISES. The performance characteristics are described by a combination of a neural network and classic correlations as presented in [17]. This work verified the new airfoils for multi-stage compressors by validating throughflow designs with 3D CFD.

A sample variation of design diffusion factor and stagger angle is depicted in figure 2 for a stator airfoil at an inlet Mach number of $M_1 = 0.67$. The figure shows qualitatively how geometry and correlations for loss and deviation adapt for different design requirements of a stator airfoil.

Throughflow Code

The throughflow calculations are performed with the streamline curvature (SLC) program ACDC developed at DLR [18]. To estimate profile loss and deviation, the code uses the calibration for the new airfoil series. In addition, correlations for 3D flow phenomena are included in the blade row model: The correlations outlined in Grieb [19] are implemented to estimate secondary losses. Tip clearance losses are computed with correlations based on the work of Denton [20] and Banjac [21]. The effect of tip clearance flow on deviation is accounted for by the deviation model of Lakshminarayana [22]. 3D deviation and losses are distributed over the blade span by functions adopted from Roberts [23]. Span-wise mixing is accounted for by a turbulent diffusion process based on the work of Gallimore [24]. The stability of the compressor is evaluated with the semi-empirical method proposed by Koch [25]. In order to achieve a convergence to a prescribed outlet pressure, a PID controller is implemented inside the throughflow code which regulates the inlet mass flow.

During the compressor design work flow, a design point computation with the throughflow code can be used to determine a subset of the design requirements for the airfoils: in each iteration of the solver, inlet Mach number, streamtube contraction and Reynolds number are extracted from the current flow solution, so that in a converged solution the blade section's operating point matches the design point of the airfoil. As the pitch-chord ratio is defined by the blade count, the axial chord and the stagger angle, the design point diffusion factor and the stagger angle remain as free parameters for each blade section. These can be prescribed directly, or outflow angle or total pressure ratio are prescribed in combination with design incidence. Design diffusion factor and stagger angle are then determined internally. Following the design point computation, the design requirements for each airfoil are fixed and off-design computations can be conducted. In a post

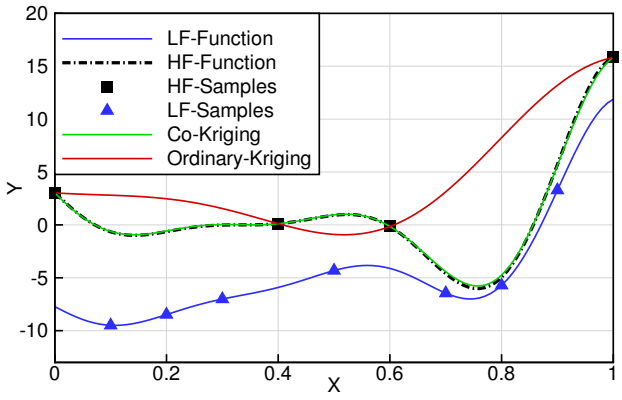

Figure 3: Analytic example that shows how low-fidelity samples can improve the prediction of a Co-Kriging model in comparison to ordinary Kriging, adopted from [28].

processing step, the interpolation routines of the VCC series in combination with a tool for blade generation can be used to create the 3D blade geometries.

Numerical Optimization

For the studies at hand the optimization suite AutoOpti [26, 27] is used. The optimizer has been developed at the DLR with focus on application in turbomachinery. An evolutionary algorithm forms the basis of the design system and creates new candidates based on mutation and differential evolution. For each variation of the design parameters a process chain is evaluated to obtain the values of objective functions and constraints. The parameter space is defined by lower and upper parameter bounds and additional nonlinear inequality constraints can be used to further restrict the feasible region. Surrogate models are used in order to improve the selection of new candidates. When generating the design parameters of a new candidate, an internal optimization on the surrogate model is conducted. For this work, 1000 sets of design parameters are analyzed before selecting the best candidate to be processed by the low or high-fidelity process chain. Only high-fidelity evaluations are ranked and act as parents in the evolutionary process. The low-fidelity evaluations are merely employed to improve the prediction of the surrogate model.

Surrogate Model

The core of the multi-fidelity support is a Co-Kriging model, which is a variant of the model published by Kennedy [29]. It was further developed at DLR and is adapted to the needs of turbomachinery design. Figure 3 demonstrates the advantage of a Co-Kriging model over ordinary Kriging. In this demonstration, an "expensive" analytic high-fidelity function is sampled at four points. The ordinary Kriging model is constructed with these high-fidelity evaluations and does not indicate where the minimum of the function lies. An additional "cheap" low-fidelity function, that serves as an estimate for the high-fidelity function is given. In this demonstration, it is merely a transformed version of the high-fidelity function. The low fidelity answers improve the prediction to a point where high-fidelity function and Co-Kriging model are very close and the optimum is described well.

More detailed information about the Co-Kriging procedure and the multi fidelity strategy can be found in [30]. The implementation for this work is characterized by the following points:

- Modern object-oriented interface-based programming language. Due to this structure it is possible to use various methods such as Ordinary-, Co-,

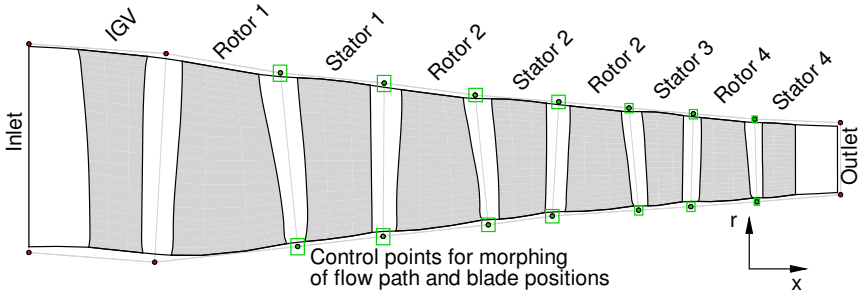

Figure 4: Initial flow path, blade positions and corresponding parameterization for optimization

Gradient-Enhanced-Kriging and also Supporting Vector Machines within one software package. This avoids redundancies and possible sources of error.

- For most Co-Kriging formulations it is necessary to calculate a low-fidelity sample at every known high-fidelity location. This is not necessary in the formulation used here.

- Numerous interfaces to modern hardware architectures have been developed. A comprehensive linear algebra library was developed, which uses Intel(c) MKL and Nvidia accelerated GPUs. In addition, an in-house OpenMP library for matrix operations can be selected and expensive numerical operations can be distributed on several computers.

- The training procedure was specially adapted and further developed for Co-Kriging. This includes the backward differentiation of the likelihood term, which leads to an acceleration of the calculation of the partial derivatives of the likelihood term. This is important for Co-Kriging, which has a very high number of parameters to be trained. Furthermore, a special training procedure for Co-Kriging was developed, which is based on a modified variant of the Resilient-Backprop-Algorithm [31] which reduces the number of evaluations of partial derivatives. In a benchmark with 230 training parameters and 400 samples, approx. 40% time could be saved. In addition, a new restart procedure was developed for Kriging training. This method evaluates trainings already carried out within an optimization and chooses the best model based on the likelihood term for the initialization of a further optimization of the likelihood. In previous tests, this procedure not only reduced the training time considerably, but also made the optimization process more stable.

SETUP OF THE OPTIMIZATION STUDY

The optimization study is performed on the test compressor DLR-Rig250 owned by the Institute of Propulsion Technology of DLR. The rig consists of four stages with two transonic front stages followed by two subsonic rear stages. The relative inlet Mach number at the tip of the front stage approaches 1.3 at nominal speed. It has been subject to numerous studies and measurement campaigns [32]. The computational domain is depicted in figure 4. For this study, the 95% and 100% relative corrected rotational speeds are analyzed. Distributions for stagnation pressure and temperature are prescribed at the inlet and the analyzed operating points are defined by their outlet pressures.

In the following, at first details on the 3D CFD setup are given, then the baseline and the initial VCC design are introduced, and finally details on the optimization setup are presented.

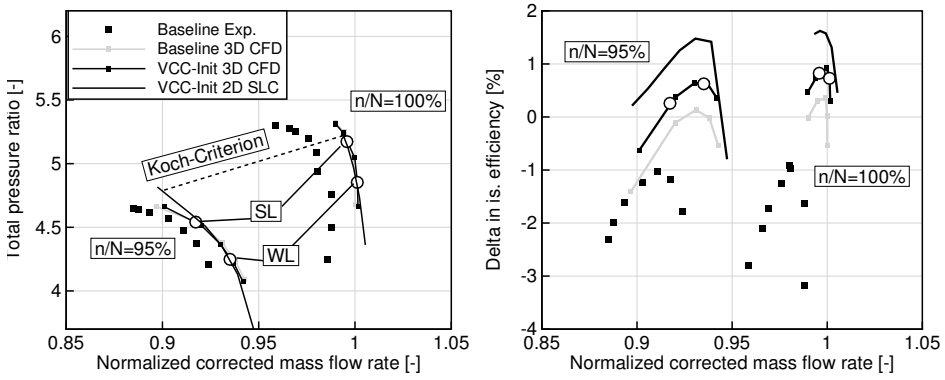

Figure 5: Compressor map of test case

Steady-state RANS Setup

The 3D CFD simulations are carried out with the solver TRACE [33, 34] which is developed at DLR for turbomachinery application. For this work, TRACE solves the steady-state Reynolds-averaged Navier-Stokes (RANS) equations using an implicit cell-centered finite volume scheme on a structured grid. The inviscid fluxes are evaluated with a Roe scheme. For space discretization the Fromm scheme is applied. For the turbulence closure the two equation Wilcox k-ω turbulence model with extensions for stagnation point anomaly and rotational effects is selected. The compressor is modeled with a single blade passage approach with mixing planes and it is discretized with a structured multi-block grid with 7.2 million cells. The span-wise resolution is 71 points with 9 points in the clearances. On all blade surfaces, the wall boundary treatment is set to wall functions. The dimensionless wall distance y^+ on the majority of the blade surfaces is between 20 and 50. All rotor blade rows have fillets. The IGV and the first two stators have semi-clearances. The two rear stators are cantilevered. As initialization, the results of the throughflow computations of the corresponding operation point are used. Convergence is achieved when the relative change in mass flow, efficiency and pressure ratio is less than 0.05% for the component, each stage and each blade row for over 500 time steps.

Baseline and Initial VCC Design

The speed lines are depicted in figure 5. Experimental results are given, as well as 3D CFD results of the baseline configuration. The baseline geometry of the compressor does not implement VCC series airfoils. For this reason, before conducting the optimization study, VCC airfoils have to be found that are comparable to the baseline airfoils. This is done by determining corresponding VCC series airfoils for five blade sections of each blade row. These airfoils are selected to have similar incidence ranges and outflow angles. In addition, the cross-sectional area is selected to be equal to the baseline airfoils. On the basis, a throughflow setup is generated and the airfoils are stacked to form a 3D geometry that is used for 3D CFD analysis. In the following, this configuration is denoted as VCC-Init. Figure 5 shows that a very good agreement in terms of total pressure ratio over mass flow rate was achieved between baseline, VCC-Init and between throughflow and 3D CFD. The compressor with the new airfoils series has a higher efficiency in comparison to the baseline design. Furthermore, the throughflow results over-predict the efficiency in comparison to the 3D CFD results.

Design Parameters

During the optimization, new design requirements are assigned to each blade section. As discussed before, only the design point diffusion factor and the stagger

angle have to be prescribed for each blade section. The other requirements are determined in a design point computation and the span-wise evolution of profile area is left untouched. The design point diffusion factor is modified in the range between 0.4 and 0.55. For the airfoils of the first rotor a change in stagger angle of 2° is allowed, for the second rotor 3° and for all other airfoils 5°. The airfoils of the last stator are selected in the throughflow code to have the same outflow angle as the baseline design. This reduces the degrees of freedom by one per stator airfoil. Each rotor and stator blade is constructed with five airfoils, so that together 75 design parameters describe the airfoils. The IGV is not modified throughout the optimizations.

In order to control the maximum stresses, shifts of the rotor airfoils in circumferential direction are included in the parameterization. For each blade four shifts are used, this makes 16 parameters.

The flow path and the blade contours are morphed based on a set of control points as depicted in figure 4. Using a two-dimensional interpolation scheme the shifts of the control points are transfered to the grid points of the flow path. The boxes in figure 4 indicate the parameter ranges. All in all, this accumulates to 119 design parameters.

Objectives and Constraints

For each compressor configuration four operating points are computed in the optimization: two operating points on the working line (WL) at 95% and 100% speed and corresponding near stall (SL) operating points.

The throughflow computations are executed in both the low and the high-fidelity process chain as the design point computation fixes the compressor geometry. Only for the high-fidelity process chain, 3D CFD computations are launched. Table 1 gives an overview on the difference between low and high-fidelity evaluation. The evaluation of the candidate geometry is only successful when all operating points reach the corresponding convergence limits.

The objectives of the optimization are the isentropic efficiencies in the two working line operating points at 95% and 100% relative speed. The mass flow rate of the 100% design point is allowed to vary by plus/minus 1% in comparison to the initial geometry. The mass flow rate of the 95% design point is not allowed to fall below the corresponding mass flow of the initial geometry.

In order to assess aerodynamic stability, the Koch stall criterion at the two near stall operating points is analyzed for the throughflow optimizations. In each operating point, the stability criterion is not allowed to decrease in comparison to the initial design. For the high-fidelity process chain the two near stall operating points merely have to converge in order to assure that the new geometry has the capability to reach at least the corresponding back pressure. For RANS simulations not converging to a stable operating point, the setup is numerically stable, so that a continuous reduction in mass flow rate can be observed as the required exit pressure cannot be achieved.

A static stress analysis is carried out for each rotor blade using geometric linear computations with quadratic 20-node brick elements using the open source finite element solver CalculiX [35]. Only the rotational forces are considered and the blades are fixed at the hub instead of including disks. The maximum Mises stress is not allowed to exceed a prescribed value.

In the end, a factor of over 2000 separates the computational time of low and high-fidelity evaluations.

RESULTS

A set of optimizations is studied to evaluate the application of throughflow and 3D CFD for compressor optimization. At first, pure throughflow optimizations are conducted and their Pareto-fronts are validated with 3D CFD. Afterwards,

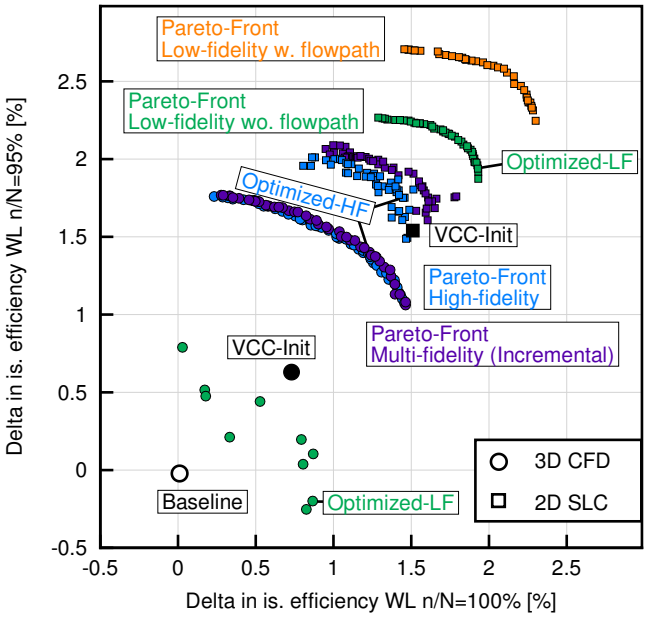

Figure 6: Pareto-fronts of optimization studies. Configurations Baseline, VCC-Init, Optimized-LF and Optimized-HF are marked. Where possible, results of low and high-fidelity process chain are given.

a reference optimization is presented, where all evaluations are done with the high-fidelity process chain. At last, the possible improvements when using multi-fidelity optimizations are investigated. As an overview, the Pareto-fronts for all optimizations are given in figure 6.

For the optimizations using the high-fidelity process chain, the hardware resources are allocated as follows: 7 computational nodes are used for 3D CFD computations and one node for the optimizer and the evaluation of the remaining process chain. This sets an upper limit of 7.5% of the computational resources for the optimizer overhead. In order to restrict the optimization overhead, low-fidelity evaluations are randomly deleted from the population in order to keep the overall number of individuals below 3000. Still, it was difficult to maintain a high load for the 3D CFD resources.

Low-Fidelity Optimizations

The low-fidelity optimizations have the advantage that they are fast and run over night. This makes them perfect to check the optimization setup including the influence of objectives and constraints on the resulting compressor map. In general, the evaluation of the process chain is very robust with almost 98% successful evaluations. Two levels of degrees of freedom are examined: with and without a modification of the flow path. For both cases around 1500 geometries are evaluated

Table 1: Characteristics of low and high fidelity process chain

	Low-fidelity	High-fidelity
Aerodynamic analysis	2D SLC	Steady-state RANS
Aerodynamic stability	Koch-criterion	Convergence
Structure analysis	fast	accurate
Computational time	0.05 CPUh	110 CPUh (converged operating point)

with the low-fidelity process chain.

Afterwards, ten configurations of the final Pareto-fronts are evaluated with the high-fidelity process chain. For the optimization with a modification of the flow path, not a single 3D CFD computation converged. This is mainly connected to unconventional design features, such as a descending hub at stator 1. The models implemented in ACDC, in this case mainly the Koch criterion, are not able to predict the aerodynamic stability for such geometries that are outside of the conventional design space. For the optimization without a modification of the flow path the points on the working line converge with 3D CFD. As a trade-off design the geometry Optimized-LF is selected for further investigations. For this configuration an increment in the working line efficiencies of 0.46% and 0.44% is predicted by the throughflow evaluations. But these improvements cannot be confirmed with 3D CFD. Instead, the improvement shrinks down to 0.17% for 100% speed and decreases by 0.83% for 95% speed. Furthermore, the operating points at the required stability limit do not converge. Accordingly, the required stability margin is not met. All in all, the high dimensional design space allows geometries that exploit the shortcomings of the throughflow model vigorously. A more thorough discussion on the errors of the implemented models for loss and deviation and the Koch stability criterion is presented below. But it becomes clear that for the presented detailed compressor optimization pure throughflow optimizations are not appropriate.

High-Fidelity Optimization

The reference optimization utilizes the high-fidelity process chain. Table 2 lists statistics for this optimization and a multi-fidelity optimization. A set of 120 geometries is computed to initialize the optimization. These are generated by mutating the initial geometry VCC-Init. Afterwards, the progress of the optimization is fast, so that the optimization converges with less than 1200 evaluated configurations. In comparison to the number of design parameters, this is less than 10-times the number of degrees of freedom. The maximum improvement in efficiency for the working line at 100% speed is 0.73% and at 95% speed it is 1.13% in comparison to configuration VCC-Init. The configuration Optimized-HF, as plotted in figure 6, is a trade-off design with similar efficiencies in both objectives. The improvements in efficiency on the working line are 0.51% for nominal speed and 0.75% for reduced speed in comparison to the VCC-Init geometry.

Multi-Fidelity Optimizations

Finally, two multi-fidelity optimizations with the methods described above are conducted denoted as “Fixed” and “Incremental”. The “Fixed” optimization utilizes a fixed set of 1200 low-fidelity evaluations. These are distributed globally at random locations in the design space. For the “Incremental” optimization, a random number generator decided on the fidelity level for the next evaluation of the process chain during the optimization. For the first 1000 geometries, 90% are evaluated with the low-fidelity process chain, afterwards the margin was decreased to 80%. For both optimizations, the same 120 high-fidelity evaluations from the

Table 2: Statistics on high and multi-fidelity optimizations

	High-fidelity (Reference)	Multi-fidelity (Incremental)
Evaluated configurations	1164	1076
Successful	98.1%	82.9%
Inside feasible region	50.3%	46.3%
Avg. area gain	1.46e-7	1.60e-7

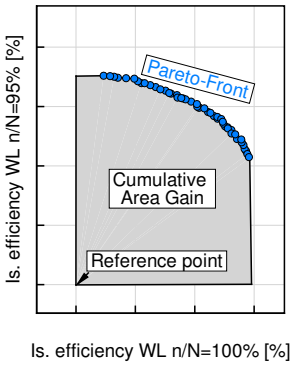

Figure 7: Definition of cumulative area gain

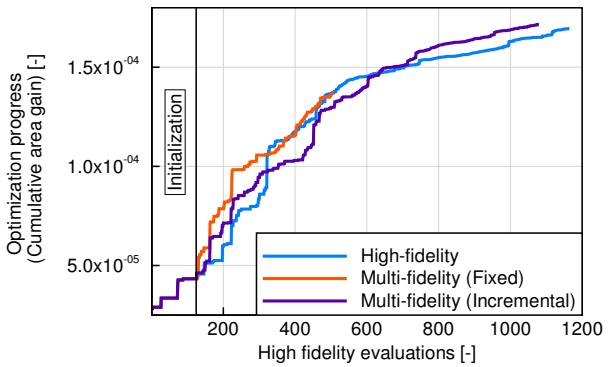

Figure 8: Optimization progress for reference and multi-fidelity optimizations in terms of cumulative area gain

reference optimization are used.

The final Pareto-fronts of the high and of the incremental multi-fidelity optimization are plotted in figure 6. Additionally, the low-fidelity evaluations of the Pareto-fronts are given. Although the high and multi-fidelity optimization have an almost identical Pareto-front on the high-fidelity side, the low-fidelity results show differences. For the high-fidelity optimization, the throughflow results do not reflect the improvements that have been made. Regarding the multi-fidelity optimization, the throughflow results show higher efficiencies in comparison to the results of the high-fidelity optimization. Accordingly, the candidate geometries resulting from the multi-fidelity optimization are more optimal on the low-fidelity level.

In order to monitor the optimization progress, a parameter called cumulative area gain is analyzed. During the optimization, the value describes the area between the current Pareto-front and user-defined barriers for each objective. It is graphically defined in figure 7. The optimization progress for the reference and the multi-fidelity optimizations in terms of the cumulative area gain is plotted over the number of high-fidelity evaluations in figure 8. Due to their high computational expense in comparison to low-fidelity evaluation and optimizer overhead, the number of high-fidelity evaluations is a reasonable measure for overall computational expense. For 200 high-fidelity evaluations after the initialization, the multi-fidelity optimizations show faster progress, afterwards the results are ambiguous. The "Fixed" optimization was aborted after 500 evaluations in favor of the "Incremental" optimization, which seemed more promising. The "Incremental" optimization reaches a comparable Pareto-Front in comparison to the high-fidelity optimization after 1022 evaluations. This is 12% less evaluations in comparison to the high-fidelity optimization. All in all, the optimization progress is similar such that a superiority of the multi-fidelity optimization cannot be ascertained. The difference can also be interpreted as random noise due to stochastic nature of the genetic optimization algorithm.

Regarding table 2, it is important to notice that in the high-fidelity optimization 98% of the high-fidelity evaluations are successful in comparison to 83% for the multi-fidelity case (Incremental). In most cases, the evaluations fail due to a divergence of the 3D CFD evaluations near the stability limit. Accordingly, the multi-fidelity optimization suffers from the high rate of geometries that do not meet the required aerodynamic stability. Presumably, the throughflow evaluations point to regions in the design space that promise high efficiencies but are aerodynamically instable. This was already observed in the low-fidelity optimizations. But the way the throughflow results contribute to the multi-fidelity optimization the Koch criterion is not considered to evaluate the aerodynamic stability.

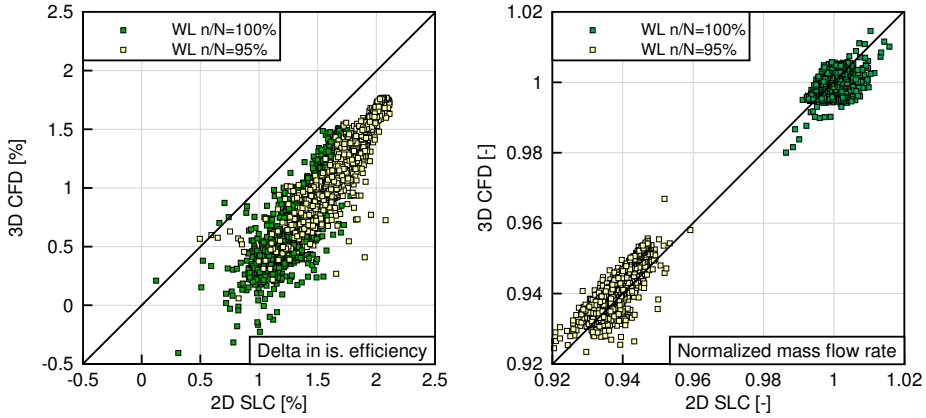

Figure 9: Correlation between 2D SLC and 3D CFD for is. efficiency and mass flow rate

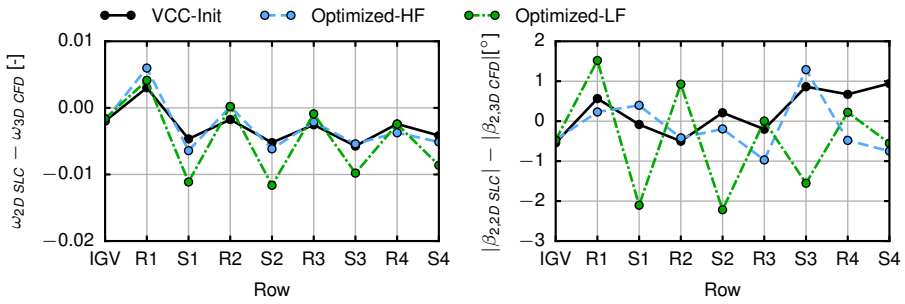

Figure 10: Differences in total pressure loss ω and relative outflow angle β_2 between 2D SLC and 3D CFD. Computed in the core flow between 33% and 67% relative channel height.

Accuracy of the Throughflow Computations

In order to get a better understanding of the shortcomings of the throughflow evaluations a more detailed comparison between the 3D CFD and the throughflow results is carried out. At first, the whole database of the multi-fidelity optimization is evaluated in figure 9 by comparing the prediction of efficiency and mass flow rate between throughflow and 3D CFD. An alignment of the data points along the main diagonal implies a perfect agreement. The more the data points are scattered, the less correlation. The efficiency predictions are not distributed around the main diagonal, instead there is a global shift to the right. This confirms a general over-prediction of efficiency by the throughflow code, which has been seen before. A global shift of this kind is corrected by the Co-Kriging model. Further deviations depend on the parameters of the individual geometries. For the mass flow rate, the two operating points are clearly separated. The error in mass flow is below 1% of normalized mass flow rate for the majority of the evaluations. All in all, the deviations are satisfactory considering that at least three orders of magnitude are between the computation times.

For a further assessment of the prediction error, the differences in total pressure loss and relative outflow angle between 2D SLC and 3D CFD are compared for the three configurations VCC-Init, Optimized-LF and Optimized-HF. The errors are computed for each blade row in the core flow between 33% and 67% relative channel height to exclude the influence of secondary flow and to focus on the output of the profile loss and deviation correlations. Starting with the total pressure loss, a clear under-prediction is observed for all blade rows except of the first transonic

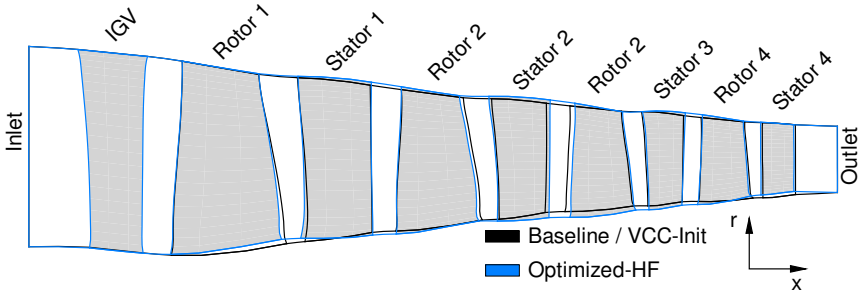

Figure 11: Initial flow path in comparison to configuration Optimized-HF

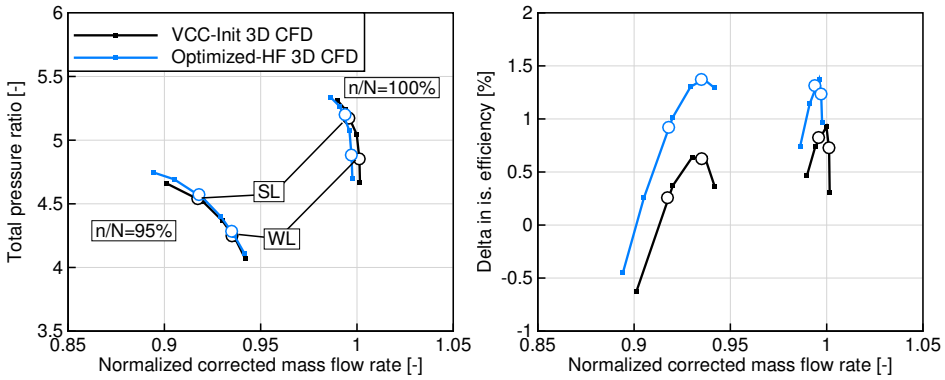

Figure 12: Compressor map comparing VCC-Init and Optimized-HF

rotor. It catches attention that errors are higher for all stator vanes in comparison to the rotor blades. The highest errors occur for the version Optimized-LF, which is optimized based on throughflow optimizations. Regarding the outflow angles for the geometries VCC-Init and Optimized-HF, the error is, with one exception, below an acceptable value of 1°. Again, the errors are significantly higher for the throughflow optimized version, with values reaching above 2° for stator 1 and 2. Accordingly, the stators of the geometry Optimized-LF are in a region of the design space where the profile correlations over-predict flow turning and under-predict the corresponding losses. This seems to be a systematic approximation error in the profile loss and deviation correlations that needs further investigation.

Analysis of Aerodynamic Improvements

The flow path and the blade positions of the version Optimized-HF are given in figure 11. The most obvious change is that the rotors have a higher and the stators a lower contraction in comparison to the baseline design. Stator 1 and 2 now have an almost constant hub line. Examining the compressor map in figure 12, the performance of the geometries Optimized-HF and VCC-Init is comparable in terms of total pressure ratio over mass flow, except that the 100% speed line is shifted to lower mass flow rates by 0.4%. This was allowed by the constraints in the optimization. The aerodynamic stability is slightly improved for the optimized version and the improvement in efficiency spans throughout both speed lines.

The stage characteristics for the version Optimized-HF and VCC-Init are presented in figure 13. The flow coefficient in the first stage is slightly reduced by the reduction in mass flow. The following three stages have a lower flow coefficient as well. This is induced by the higher work input in the front stage and the increased flow area in front of the rotors. For the work coefficient, the most obvious change is that work input is moved from the second rotor to the first. The reaction coefficient drops for the last three stages, this means more load is put onto

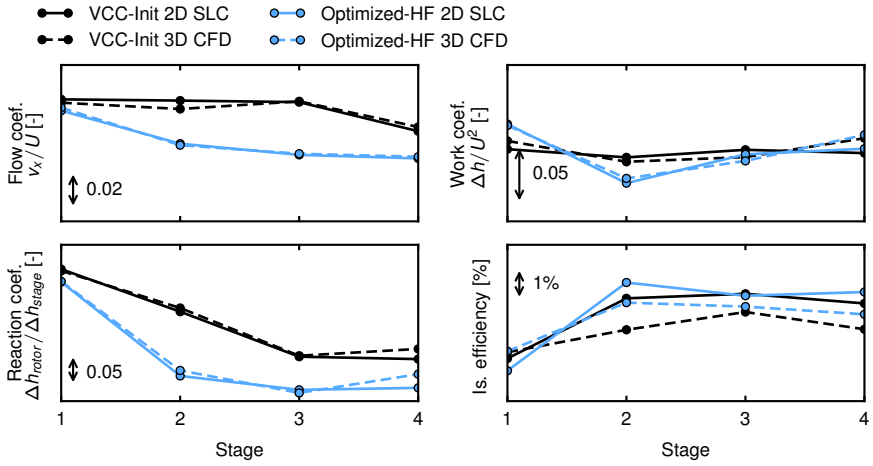

Figure 13: Stage characteristics comparing configuration Optimized-HF to VCC-Init for 100% speed on the working line

the stators. Meanwhile the stagger increases and camber decreases in the stators as reflected by the geometry. The 3D CFD results suggest an equal or higher efficiency of the optimized version for all stages with hardly any improvements in stage 1 and largest improvements in stage 2. This seems to be a key factor in the design: increasing the work input in stage 1 while maintaining the efficiency and lowering the work input in stage 2 to gain high efficiency there. Comparing throughflow results and 3D CFD, both are in good accordance for flow, work and reaction coefficient. The trend of the throughflow results to over-predict efficiency is reflected in the stage-wise results as well.

The isentropic Mach number distribution on the blade suction sides is visualized for VCC-Init and Optimized-HF in figure 14. These results confirm the observations in the stage characteristics: with higher work input, the pre-shock Mach number in the first rotor increases, whereas the maximum Mach numbers in the following three rotors decrease. In particular the shock in the second rotor is reduced significantly. In the VCC-Init design, the shock spans over a large part of the radial height in comparison to the Optimized-HF design where the shock is limited to the upper part of the blade.

CONCLUSION

This paper presents a study on the use of throughflow and 3D CFD in a multi-fidelity optimization environment. The high-fidelity reference optimization is characterized by a fast optimization progress with less than 1200 evaluations for around 120 design parameters. In comparison to the baseline design, the isentropic efficiency for the working line point on the 100% speed line is increased by 1.24% and for the 95% speed line by 1.37%. Compressor geometries that are optimized purely with throughflow evaluations have considerable aerodynamic stability issues. This confirms Casey's [4] statement that preliminary design methods are not suitable for numerical optimization. In the multi-fidelity optimization, the throughflow computations contributed to the optimization progress in a limited way. At the beginning of the optimization a faster progress is possible, but a high rate of non-convergence of the 3D CFD computation slowed down the optimization progress in the later phase. The throughflow results point to regions in the design space that promise high efficiencies but do not meet the requirements for aerodynamic stability. In this work, the 0D Koch criterion is employed in the throughflow optimizations to assess stability, but in the investigated scenario it performs poorly. In the end, the criterion is based on a simple diffuser analogy

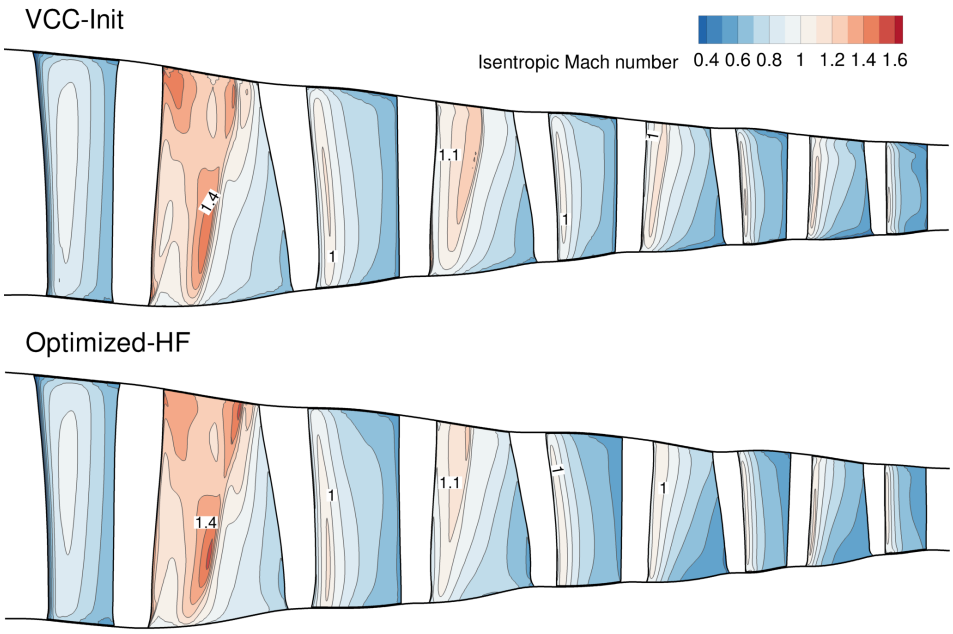

Figure 14: Isentropic Mach number distribution on blade suction sides. The values are computed based on a reference stagnation pressure which is extracted from mixing planes upstream of each blade row at corresponding radial heights.

and although it can give good results for well-design compressors it fails to assess unconventional designs created in an optimization process. The authors share the opinion that further improvements to the throughflow model and the handling in the optimization procedure can make the throughflow predictions more valuable in a multi-fidelity setup. For example, a more elaborate model for stability that considers span-wise variations, such as the model presented in [21], may be of help. The optimization of a compressor with additional stages puts more focus on axial matching and might increase the relevance of the throughflow results as well. Furthermore, it has to be stressed that the baseline compressor is already very efficient. Accordingly, the presented optimization focuses on flow details, which are difficult to assess by the throughflow code.

Anyhow, the application of the throughflow code is indispensable in the presented design work flow as it contributes to the selection of the compressor airfoils from the airfoil series in a design point computation. All of the presented optimizations benefit from the new airfoil series that is able to reduce the amount of compressor design parameters significantly. Including modifications of the duct, only 120 parameters are necessary to describe eight blade rows. A comparison to an optimization with a detailed airfoil parameterization based on B-Spline curve parameters might be valuable, but is very expensive. Assuming 10 degrees of freedom per airfoil, the overall number of design parameters would exceed 400.

REFERENCES

[1] Hearsey, R. M., 1989. "Numerical optimization of axial compressor designs". *ASME Paper No. 89-GT-14.*

[2] Oyama, A., and Liou, M.-S., 2002. "Multiobjective optimization of a multi-stage compressor using evolutionary algorithm". *AIAA paper No. 2002-3545.*

[3] Joly, M., Verstraete, T., and Paniagua, G., 2012. "Full design of a highly loaded fan by multi-objective optimization of through-flow and high-fidelity aero-mechanical performances". *ASME Paper No. GT2012-69686.*

[4] Casey, M., 1994. "Computational Methods for Preliminary Design and Geometry Definition in Turbomachinery". In Turbomachinery Design Using CFD, no. AGARD-LS-195.

[5] Benini, E., 2004. "Three-dimensional multi-objective design optimization of a transonic compressor rotor". *Journal of propulsion and power,* ***20***(3), pp. 559–565.

[6] Li, H.-D., He, L., Li, Y., and Wells, R., 2006. "Blading aerodynamics design optimization with mechanical and aeromechanical constraints". *ASME Paper No. GT2006-90503*, pp. 1319–1328.

[7] Siller, U., and Aulich, M., 2010. "Multidisciplinary 3D-Optimization of a Fan Stage Performance Map With Consideration of the Static and Dynamic Rotor Mechanics". *ASME Paper No. GT2010-22792.*

[8] Baert, L., Lepot, I., Sainvitu, C., Chérière, E., Nouvellon, A., and Leonardon, V., 2019. "Aerodynamic optimisation of the low pressure turbine module: Exploiting surrogate models in a high-dimensional design space". *ASME Paper No. GT2019-91570.*

[9] Brooks, C. J., Forrester, A. I. J., Keane, A. J., and Shahpar, S., 2011. "Multi-Fidelity Design Optimisation of a Transonic Compressor Rotor". *9th European Conf. Turbomachinery Fluid Dynamics and Thermodynamics, Istanbul, Turkey.*

[10] Reid, L., and Moore, R. D., 1978. "Design and overall performance of four highly loaded, high speed inlet stages for an advanced high-pressure-ratio core compressor".

[11] Lapworth, L., and Shahpar, S., 2004. "Design of Gas Turbine Engines Using CFD". *European Congress on Computational Methods in Applied Sciences and Engineering ECCOMAS 2004.*

[12] Meillard, L., Mihail Stanica, W., Ben Nasr, N., and Riéra, W., 2017. "Design of a counter rotating fan using a multidisciplinary and multifidelity optimisation under high level of restrictions". In ISABE 2017.

[13] Schnoes, M., and Nicke, E., 2017. "Exploring a Database of Optimal Airfoils for Axial Compressor Design". In ISABE 2017, no. ISABE-2017-21493.

[14] Köller, U., Mönig, R., Küsters, B., and Schreiber, H.-A., 2000. "Development of Advanced Compressor Airfoils for Heavy-Duty Gas Turbines - Part I: Design and Optimization". *ASME J. Turbomach,* ***122***(3), pp. 397–405.

[15] Drela, M., and Youngren, H., 1998. *A User's Guide to MISES 2.53.* MIT Aerospace Computational Design Laboratory, Cambridge, MA, United States.

[16] Matheron, G., 1963. "Principles of Geostatistics". *Economic Geology,* ***58***(8), pp. 1246–1266.

[17] Schnoes, M., Voß, C., and Nicke, E., 2018. "Design Optimization of a Multi-Stage Axial Compressor Using Throughflow and a Database of Optimal Airfoils". *Journal of the Global Power and Propulsion Society,* ***2***, pp. 516–528.

[18] Schmitz, A., Aulich, M., Schönweitz, D., and Nicke, E., 2012. "Novel Performance Prediction of a Transonic 4.5-Stage Compressor". *ASME Paper No. GT2012-69003.*

[19] Grieb, H., Schill, G., and Gumucio, R., 1975. "A Semi-Empirical Method for the Determination of Multistage Axial Compressor Stage Efficiency". *ASME Paper No. 75-GT-11.*

[20] Denton, J. D., and Cumpsty, N., 1993. "Loss mechanisms in turbomachines". *ASME J. Turbomach,* ***115***(4), pp. 621–656.

[21] Banjac, M., Petrovic, V., and Wiedermann, A., 2015. "Secondary Flows, Endwall Effects and Stall Detection in Axial Compressor Design". *ASME J. Turbomach,* ***137***(5), p. 051004.

[22] Lakshminarayana, B., 1970. "Methods of Predicting the Tip Clearance Effects in Axial Flow Turbomachinery". *ASME J. Basic Eng.,* ***92***(3), pp. 467–482.

[23] Roberts, W. B., Serovy, G. K., and Sandercock, D. M., 1986. "Modeling the 3-D Flow Effects on Deviation Angle for Axial Compressor Middle Stages". *ASME J. Eng. Gas Turbines Power,* ***108***(1), pp. 131–137.

[24] Gallimore, S. J., 1986. "Spanwise Mixing in Multistage Axial Flow Compressors: Part II - Throughflow Calculations Including Mixing". *ASME J. Turbomach,* ***108***(1), pp. 10–16.

[25] Koch, C. C., 1981. "Stalling pressure rise capability of axial flow compressor stages". *ASME J. Eng. Power,* ***103***(4), pp. 645–656.

[26] Aulich, M., Voss, C., and Raitor, T., 2014. "Optimization Strategies demonstrated on a Transonic Centrifugal Compressor". *ISROMAC 15.*

[27] Voß, C., Aulich, M., and Raitor, T., 2014. "Metamodel Assisted Aeromechanical Optimization of a Transonic Centrifugal Compressor". *ISROMAC 15.*

[28] Forrester, A. I., Sóbester, A., and Keane, A. J., 2007. "Multi-fidelity optimization via surrogate modelling". *Proceedings of the royal society a: mathematical, physical and engineering sciences,* ***463***(2088), pp. 3251–3269.

[29] Kennedy, M. C., and O'Hagan, A., 2000. "Predicting the output from a complex computer code when fast approximations are available". *Biometrika,* ***87***, pp. 1–13.

[30] Schmitz, A., 2019. "Multifidelity-optimierungsverfahren für turbomaschinen". Dissertation, Ruhr Universität Bochum.

[31] Riedmiller, M., and Braun, H., 1993. "A direct adaptive method for faster backpropagation learning: The RPROP algorithm". In Neural Networks, 1993., IEEE International Conference on, IEEE, pp. 586–591.

[32] Schönweitz, D., Voges, M., Goinis, G., Enders, G., and Johann, E., 2013. "Experimental and Numerical Examinations of a Transonic Compressor-Stage With Casing Treatment". *ASME Paper No. GT2013-95550.*

[33] Kügeler, E., Weber, A., Nürnberger, D., and Engel, K., 2008. "Influence of Blade Fillets on the Performance of a 15 Stage Gas Turbine Compressor". *ASME Paper No. GT2008-50748.*

[34] Becker, K., Heitkamp, K., and Kügeler, E., 2010. "Recent Progress in a Hybrid-Grid CFD Solver for Turbomachinery Flows". *ECCOMAS CFD 2010.*

[35] Dhondt, G., 2004. *The finite element method for three-dimensional thermomechanical applications.* John Wiley & Sons.